

Classical variational simulation of the Quantum Approximate Optimization Algorithm

Matija Medvidović

Center for Computational Quantum Physics, Flatiron Institute,

162 5th Avenue, New York, NY 10010, USA and

Department of Physics, Columbia University, New York 10027, USA

Giuseppe Carleo

Institute of Physics, École Polytechnique Fédérale de Lausanne (EPFL), CH-1015 Lausanne, Switzerland

A key open question in quantum computing is whether quantum algorithms can potentially offer a significant advantage over classical algorithms for tasks of practical interest. Understanding the limits of classical computing in simulating quantum systems is one key route to address this question. In this work we introduce a method to classically simulate quantum circuits consisting of several layers of parametrized gates, a key component of many variational quantum algorithms suitable for near-term quantum computers. The classical simulation approach we adopt is based on a neural-network quantum state parametrization of the many-qubit wave function. As a specific example, we focus on alternating layered ansatz states that are relevant for the Quantum Approximate Optimization Algorithm (QAOA). For the largest circuits simulated, we reach 54 qubits and 20 layers of independent gates (depth) without requiring large-scale computational resources. When available, we compare the obtained states with outputs of exact simulators and find good approximations for both the cost function values and state vectors. For larger number of qubits, our approach can be used to provide accurate simulations of QAOA at previously unexplored regions of its parameter space, and to benchmark the next generation of experiments in the Noisy Intermediate-Scale Quantum (NISQ) era.

I. INTRODUCTION

The past decade has seen a fast development of quantum technologies and the achievement of an unprecedented level of control in quantum hardware [1], clearing the way for demonstrations of quantum computing applications for practical uses. However, near-term applications face some of the limitations intrinsic to the current generation of quantum computers, often referred to as Noisy Intermediate-Scale Quantum (NISQ) hardware [2]. In this regime, a limited qubit count and absence of quantum error correction constrain the kind of applications that can be successfully realized. Despite these limitations, hybrid classical-quantum algorithms [3–6] have been identified as the ideal candidates to assess the first possible advantage of quantum computing in practical applications.

The Quantum Approximate Optimization Algorithm (QAOA) [5] is a notable example of variational quantum algorithm with prospects of quantum speedup on near-term devices. Devised to take advantage of quantum effects to solve combinatorial optimization problems, it has been extensively theoretically characterized [7–12], and also experimentally realized on state-of-the-art NISQ hardware [13]. While the general presence of quantum advantage in quantum optimization algorithms remains an open question [14–16], QAOA has gained popularity as a quantum hardware benchmark [17–20]. As its desired output is essentially a classical state, the question arises whether a specialized classical algorithm can efficiently simulate it [21], at least near the variational optimum.

In this paper, we use a classical variational

parametrization of the many-qubit state based on Neural Network Quantum States (NQS) [22] and extend the method of Ref. [23] to simulate QAOA. This approach trades the need for exact *brute force* exponentially scaling classical summation with an approximate, yet accurate, classical variational description of the quantum circuit. In turn, we obtain an heuristic classical method that can significantly expand the possibilities to simulate NISQ-era quantum optimization algorithms. We successfully simulate the Max-Cut QAOA circuit [5, 7, 13] for 54 qubits at depth $p = 4$ and use the method to perform a variational parameter sweep on a 1D cut of the parameter space. The method is contrasted with state-of-the-art classical simulations based on low-rank Clifford group decompositions [21], whose complexity is exponential in the number of non-Clifford gates as well as tensor-based approaches [24]. Instead, limitations of the approach are discussed in terms of the QAOA parameter space and its relation to different initializations of the stochastic optimization method used in this work.

II. QUANTUM APPROXIMATE OPTIMIZATION ALGORITHM

The Quantum Approximate Optimization Algorithm (QAOA) [5, 8] is a variational quantum algorithm for approximately solving discrete combinatorial optimization problems. In this work, we study a quadratic cost function associated with a MaxCut problem on graphs.

If we consider a graph G and denote the set of its edges by $E(G)$, the MaxCut of the graph G is defined by the

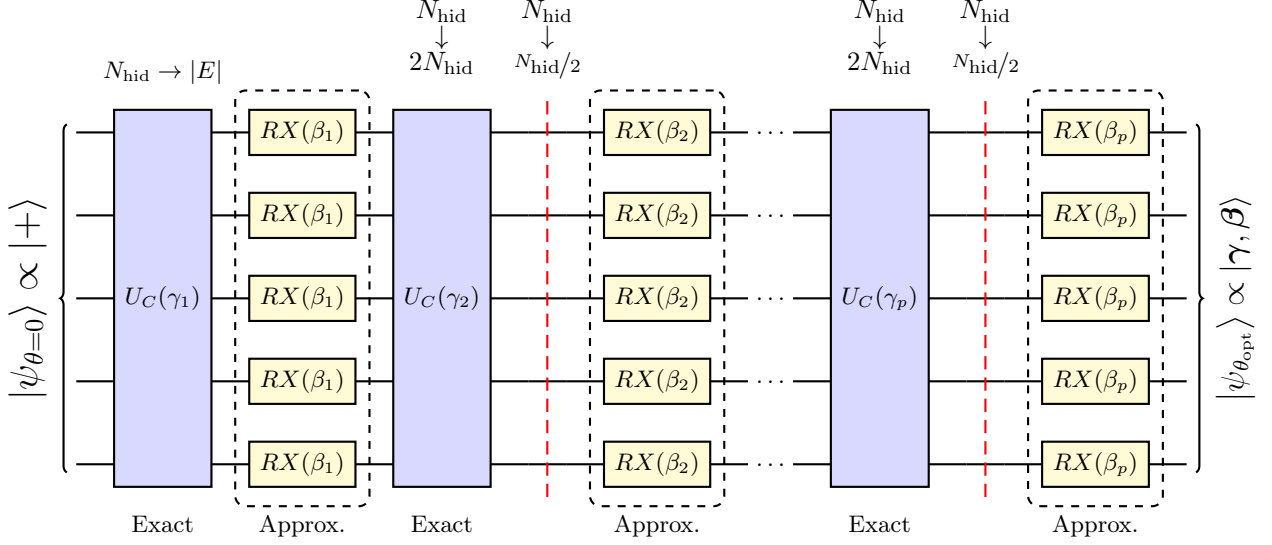


FIG. 1. **A schematic representation of the QAOA circuit and our approach to simulating it.** The input state is trivially initialized to $|+\rangle$. Next, at each p , the exchange of exactly (U_C) and approximately ($RX(\beta) = e^{-i\beta X}$) applicable gates is labeled (See Appendix A). As noted in the main text, each (exact) application of the U_C gate leads to an increase in the number of hidden units by $|E|$ (the number of edges in the graph). In order to keep that number constant, we "compress" the model, indicated by red dashed lines after each U_C gate. The compression is repeated at each layer after the first, halving the number of hidden units each time, immediately after doubling it with U_C gates. After the final layer, the RBM is parametrized by θ_{opt} , approximating the final QAOA target state $|\gamma, \beta\rangle$.

following operator:

$$\mathcal{C} = \sum_{i,j \in E(G)} w_{ij} Z_i Z_j, \quad (1)$$

where w_{ij} are the edge weights. The classical bitstring \mathcal{B} that minimizes $\langle \mathcal{B} | \mathcal{C} | \mathcal{B} \rangle$ is the graph partition with the maximum cut. QAOA approximates such a quantum state through a quantum circuit of predefined depth p :

$$|\gamma, \beta\rangle = U_B(\beta_p) U_C(\gamma_p) \cdots U_B(\beta_1) U_C(\gamma_1) |+\rangle, \quad (2)$$

where $|+\rangle$ is a symmetric superposition of all computational basis states: $|+\rangle = H^{\otimes N} |0\rangle^{\otimes N}$ for N qubits. The set of $2p$ real numbers γ_i and β_i for $i = 1 \dots p$ define the variational parameters to be optimized over by an external classical optimizer. The unitary gates defining the parametrized quantum circuit read $U_B(\beta) = \prod_{i \in G} e^{-i\beta X_i}$ and $U_C(\gamma) = e^{-i\gamma \mathcal{C}}$.

Optimal variational parameters γ and β are then found through an outer-loop classical optimizer of the following quantum expectation value:

$$C(\gamma, \beta) = \langle \gamma, \beta | \mathcal{C} | \gamma, \beta \rangle \quad (3)$$

In this work we consider 3-regular graphs with all weights w_{ij} set to unity at QAOA depths of $p = 1, 2, 4$. At $p = 1$, we base our parameter choices on the position of global optimum that can be computed exactly (see Appendix C). For $p = 2$ and $p = 4$, we resort to direct numerical evaluation of the cost function as given

in Eq. 1 from either the complete state vector of the system (number of qubits permitting) or from importance-sampling the output state as represented by a Restricted Boltzmann Machine. For all p , we find the optimal angles using Adam [25] with either numerical or exact gradients.

III. CLASSICAL SIMULATION

Consider a quantum system consisting of N qubits. The Hilbert space is spanned by the computational basis $\{|\mathcal{B}\rangle : \mathcal{B} \in \{0, 1\}^N\}$ of classical bit strings $\mathcal{B} = (B_1, \dots, B_N)$. A general state can be expanded in this basis as $|\psi\rangle = \sum_{\mathcal{B}} \psi(\mathcal{B}) |\mathcal{B}\rangle$. The convention $Z_i |\mathcal{B}\rangle = (-1)^{B_i} |\mathcal{B}\rangle$ is adopted. We use a neural-network representation of the many-body wavefunction $\psi(\mathcal{B})$ associated with this system, and specifically adopt a shallow network of the Restricted Boltzmann Machine (RBM) type: [26–28]

$$\begin{aligned} \psi(\mathcal{B}) \approx \psi_{\theta}(\mathcal{B}) &\equiv \exp \left(\sum_{j=1}^N a_j B_j \right) \cdot \\ &\cdot \prod_{k=1}^{N_h} \left[1 + \exp \left(b_k + \sum_{j=1}^{N_v} W_{jk} B_j \right) \right]. \end{aligned} \quad (4)$$

The RBM provides a classical variational representation of the quantum state [22], and is parametrized by a set of complex parameters $\theta = \{\mathbf{a}, \mathbf{b}, W\}$ – visible biases

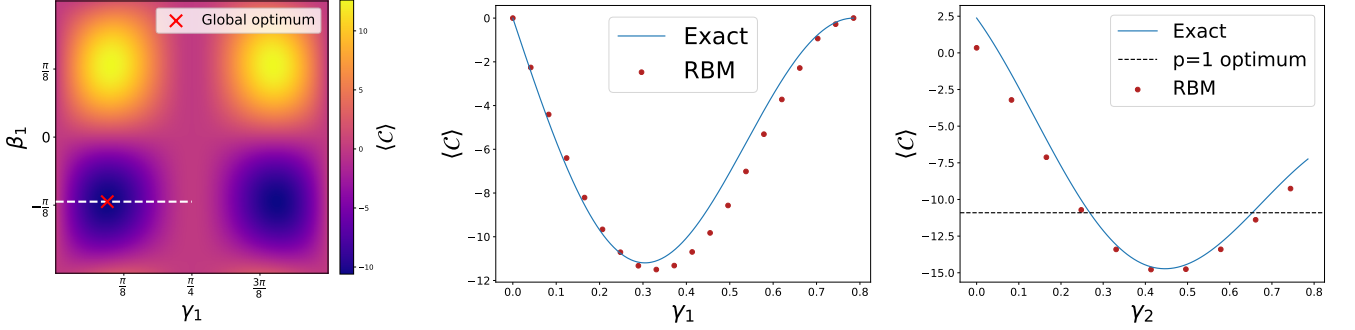


FIG. 2. **Left:** The exact variational QAOA landscape at $p = 1$ of a random 20-qubit instance of a 3-regular graph is presented, calculated using the analytical cost formula (see Appendix C). The optimum was found using a gradient-based optimizer [25] and marked. The restricted cut along the constant- β line and at optimal γ is more closely studied in the center panel. **Center:** RBM-based output wavefunctions are contrasted with exact results. **Right:** A similar variational landscape cut is presented at $p = 2$. Optimal $p = 2$ QAOA parameters are calculated using numerical derivatives and a gradient-based optimizer. Parameters γ_1, β_1 and β_2 are fixed at their optimal values while the cost function γ_2 -dependence is investigated. We note that our approach is able to accurately reproduce the increased proximity to the combinatorial optimum associated with increasing QAOA depth p .

$\mathbf{a} = (a_1, \dots, a_N)$, hidden biases $\mathbf{b} = (b_1, \dots, b_{N_h})$ and weights $W = (W_{j,k} : j = 1 \dots N, k = 1 \dots N_h)$. The complex-valued ansatz given in Eq. 4 is, in general, not normalized.

We note that the N -qubit $|+\rangle$ state required for initializing QAOA can always be exactly implemented by setting all variational parameters to 0. That choice ensures that the wavefunction ansatz given in Eq. 4 is constant across all computational basis states, as required. The advantage of using the ansatz given in Eq. 4 as an N -qubit state is that a subset of one- and two-qubit gates can be exactly implemented as mappings between different sets of variational parameters $\theta \mapsto \theta'$. In general, such mapping corresponding to an abstract gate \mathcal{G} is found as the solution of the following nonlinear equation:

$$\langle \mathcal{B} | \psi_{\theta'} \rangle = C \langle \mathcal{B} | \mathcal{G} | \psi_{\theta} \rangle, \quad (5)$$

for all bitstrings \mathcal{B} and any constant C , if a solution exists. For example, consider the Pauli Z gate acting on qubit i . In that case, Eq. 5 reads $e^{a'_i B_i} = C(-1)^{B_i} e^{a_i B_i}$ after trivial simplification. The solution is $a'_i = a_i + i\pi$ for $C = 1$, with all other parameters remaining unchanged. Such replacement rules for all three Pauli gates are discussed in the Appendix A. In addition, one can exactly implement a subset of two-qubit gates by introducing an additional hidden unit coupled only to the two qubits in question. Labeling the new unit by c , we can implement the RZZ gate relevant for QAOA. The gate is given as $RZZ(\phi) = e^{-i\phi Z_i Z_j} \propto \text{diag}(1, e^{i\phi}, e^{i\phi}, 1)$ up to a global phase. The replacement rules read:

$$\begin{aligned} W_{ic} &= -2\mathcal{A}(\phi), & W_{jc} &= 2\mathcal{A}(\phi) \\ a_i &\rightarrow a_i + \mathcal{A}(\phi), & a_j &\rightarrow a_j - \mathcal{A}(\phi), \end{aligned} \quad (6)$$

where $\mathcal{A}(\phi) = \text{Arccosh}(e^{i\phi})$ and $C = 2$. Derivations of replacement rules for these and other gates can be found in Appendix A.

Not all gates can be applied through solving Eq. 5. Most notably, gates that form superpositions belong in this category, including $U_B(\beta) = \prod_i e^{-i\beta X_i}$ required for running QAOA. This happens simply because a linear combination of two or more RBMs cannot be exactly represented by a single new RBM through a simple variational parameter change. To simulate those gates, we employ a variational stochastic optimization scheme.

We take $\mathcal{D}(\phi, \psi) = 1 - F(\phi, \psi)$ as a measure of distance between two arbitrary quantum states $|\phi\rangle$ and $|\psi\rangle$, where $F(\phi, \psi)$ is the usual quantum fidelity:

$$F(\phi, \psi) = \frac{|\langle \phi | \psi \rangle|^2}{\langle \phi | \phi \rangle \langle \psi | \psi \rangle}, \quad (7)$$

In order to find variational parameters θ which approximate a target state $|\phi\rangle$ well ($|\psi_{\theta}\rangle \approx |\phi\rangle$, up to a normalization constant), we minimize $\mathcal{D}(\psi_{\theta}, \phi)$ using a gradient-based optimizer. In this work we use the Stochastic Re-configuration (SR) [29] algorithm to achieve that goal.

For larger p , extra hidden units introduced $U_C(\gamma)$ at each layer can result in a large number of associated parameters to optimize over that are not strictly required for accurate output state approximations. So keep the parameter count in check, we insert a model *compression* step which halves the number of hidden units immediately after applying U_C doubles it. Specifically we create an RBM with fewer hidden units and fit it to the output distribution of the larger RBM (output of U_C). Exact circuit placement of compression steps are shown on Fig. 1 and details are provided in Appendix B 2.

IV. RESULTS

In this section we present our simulation results for 20- and 54-qubit instances of QAOA. In addition we discuss

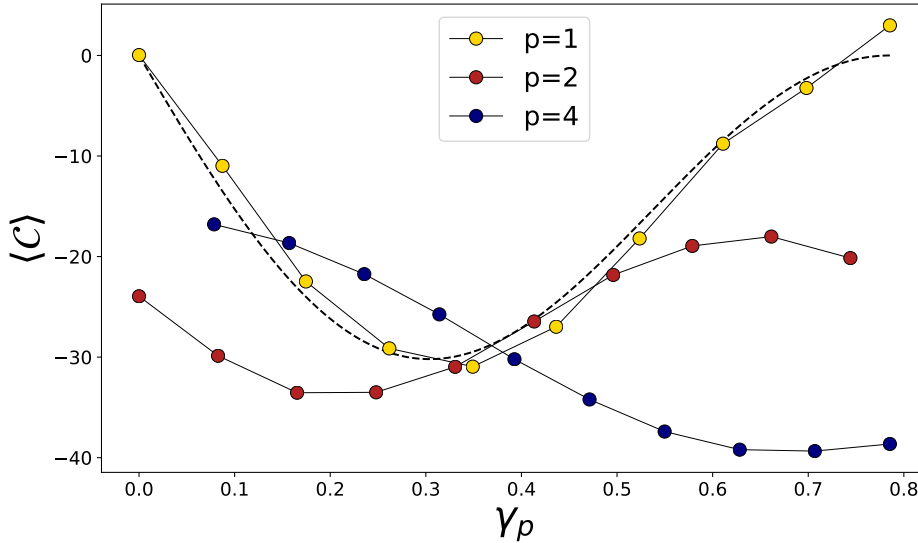


FIG. 3. Randomly generated 3-regular graphs with 54 nodes are considered at $p = 1, 2, 4$. At each p , all angles were set to optimal values for a different graph of 20 nodes, except for the final γ_p . Cost dependence along this 1D slice of the variational landscape (a higher-dimensional analogue of the leftmost panel of Fig. 2) is investigated. Data points are calculated using MCMC sampling and compared to exact results available through an analytical formula (see Appendix C) at $p = 1$ (dashed curve). Error bars were calculated using bootstrap resampling but were too small to be visible on the plot. At $p = 2$, this 54-qubit simulation approximately implements 162 RZZ gates and 108 RX gates while at $p = 4$ there are 324 RZZ s and 216 RX s. Despite non-optimal angles, our model was able to capture the overall better QAOA approximation of the actual combinatorial optimum. A tight upper bound on that optimum was calculated to be $C_{\text{opt}} \lesssim -69$ by directly optimizing an RBM to represent a ground state of the cost operator in Eq. 3

model limitations and its relation to current state-of-the-art simulations.

We begin by studying the performance of our approach on a 20-qubit system corresponding to the MaxCut problem on a 3-regular graph of order 20. In that case, access to exact numerical wavefunctions is not yet severely restricted by the number of qubits. That makes it a suitable test-case. The results can be found on Fig. 2.

In Fig. 2, we can see that our approach reproduces variations in the cost landscape associated with different choices of QAOA angles at both $p = 1$ and $p = 2$. At $p = 1$, an exact formula (see Appendix C) is available for comparison of cost function values. We report that, at optimal angles, the overall final fidelity (overlap squared) was consistently above 0.94 for all random graph instances we simulated. Single-qubit fidelities were found to be > 0.99 almost universally. However, we find that the stochastic optimization performance seems to be sensitive to choices of QAOA variational parameters γ and β away from optimum (see Fig. 4 and accompanying discussion).

For the 54 qubit case, results can be seen on Fig. 3. We approximately reproduce the exact error curve (see Appendix C), implementing 81 RZZ ($e^{-i\gamma Z \otimes Z}$) gates exactly and 54 RX ($e^{-i\beta X}$) gates using the described optimization method. We perform QAOA at $p = 2$ and $p = 4$ for the 54-qubit graph as well. Given that RZZ gates do not belong to the Clifford group, this simulation is the first

classical implementation of QAOA on a system of this size, to the best of our knowledge, for $p = 1$, $p = 2$ and $p = 4$. Specifically at $p = 4$, we approximately implement 324 RZZ gates, greatly exceeding the capabilities of modern exact simulators. Given the favorable scaling of our approach with system size near the optimum, we conjecture that it may be used for even larger systems or larger QAOA depths p to investigate previously unknown regions of the QAOA cost landscape.

Next, we discuss our model performance for points in the QAOA cost landscape away from optimum. In general, we report that overall fidelity between the state represented by our RBM ansatz (Eq. 4) and the exact N -qubit state decreases one departs from exactly reproducible states by changing γ and β . By *exactly reproducible*, we mean the initial state $|+\rangle$ and all states related to it through applications of gates that can be exactly applied to the RBM ansatz. (See Appendix A).

In the case of QAOA on 3-regular graphs, we notice that the fidelity decreases as relevant parameters are increased beyond the optimum. The situation is shown on Fig. 4. Therefore, this model is less accurate when studying QAOA states away from the variational optimum. However, even in regions with lowest fidelities, RBM-based QAOA states are able to approximate cost well, as can be seen in Fig. 2 and Fig. 3.

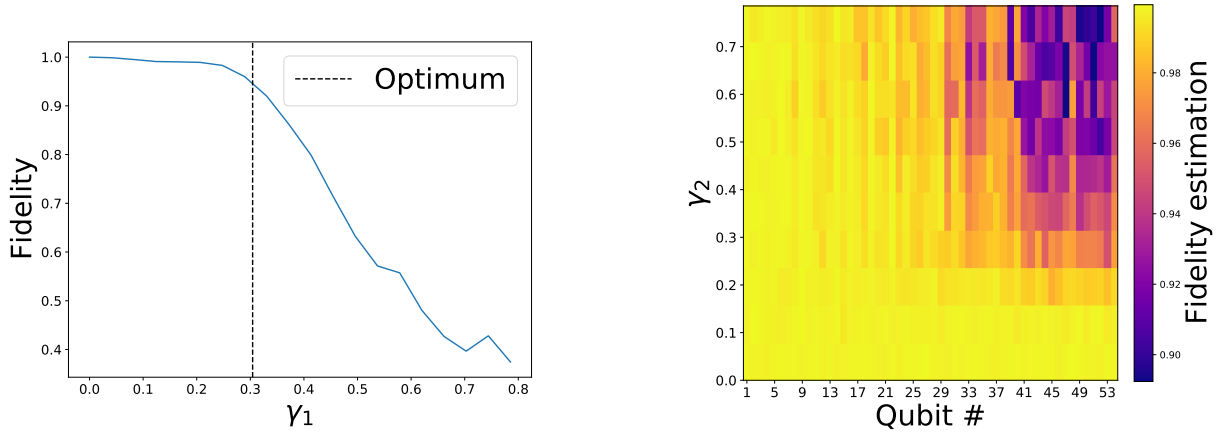


FIG. 4. **Left:** A comparison between the exact fidelity between the full RBM-ansatz wavefunction and the exact simulation results are shown for a 20 qubit system at $p = 1$. β was kept at its optimal value. We note that the fidelity begins to significantly drop approximately as γ increases beyond the optimal value. **Right:** An array of final stochastic estimations of single-qubit fidelities (see Appendix B1 for formula) in the course of optimizer progress. The system presented consists of 54 qubits at $p = 2$ where exact state vectors are intractable for direct comparison. A similar qubit-by-qubit trend can be noticed across all system sizes and depths p we studied.

1. Comparison with other methods

In modern sum-over-Cliffords/Metropolis simulators, computational complexity grows exponentially with the number of non-Clifford gates. With the *RZZ* gate being a non-Clifford operation, even our 20-qubit toy example, exactly implementing 60 *RZZ* gates at $p = 2$, is approaching the limit of what those simulators can do [21]. In addition, that limit is greatly exceeded by the larger, 54-qubit system we study next, implementing 162 *RZZ* gates. State-of-the-art tensor-based approaches [24] have been used to simulate larger circuits but are ineffective in the case of non-planar graphs.

Another very important tensor-based method is the Matrix Product State (MPS) variational representation of the many-qubit state. This is a low-entanglement representation of quantum states, whose accuracy is controlled by the so-called bond-dimension. Routinely adopted to simulate ground states of one-dimensional systems with high accuracy [30–32], extensions of this approach to simulate challenging circuits have also been recently put forward [33]. In Fig. 5, our approach is compared with an MPS ansatz. We establish that for small systems, MPS provides reliable results with relatively small bond dimensions. For larger systems, however, our approach significantly outperforms MPS-based circuit simulation methods both in terms of memory requirements (fewer parameters) and overall runtime. This is to be expected in terms of entanglement capacity of MPS wave functions, that are not specifically optimized to handle non-one dimensional interaction graphs, as in this specific case at hand. For a more direct comparison, we estimate the MPS bond dimension required for reaching RBM performance at $p = 2$ and 54 qubits to be $\sim 10^4$ (see Fig. 5), amounting to $\sim 10^{10}$ complex param-

eters (≈ 160 GB of storage) while our RBM approach uses ≈ 4500 parameters (≈ 70 kB of storage). In addition, we expect the MPS number of parameters to grow with depth p because of additional entanglement, while RBM sizes heuristically scale weakly with p and can be controlled mid-simulation using our compression step.

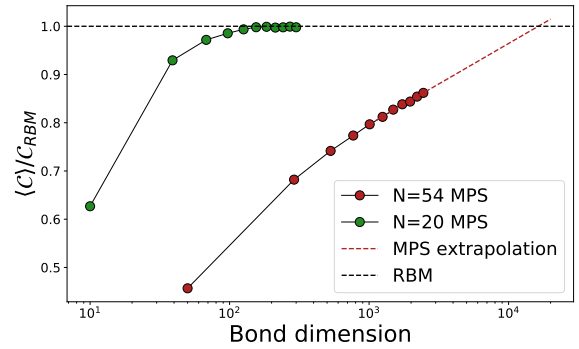


FIG. 5. A range of MPS-based QAOA simulations are compared to our RBM ansatz performance on both 20-qubit and 54-qubit graphs at $p = 2$. In the 20-qubit case, we see quick convergence to the QAOA cost optimum with increasing bond dimension. Approximation ratio with of the RBM output is shown on the y-axis. However, on a 54-qubit graph, MPS accuracy increases approximately logarithmically with bond dimension. An approximation of the MPS bond dimension required for reaching RBM performance is extrapolated to be $\approx 1.5 \times 10^4$ which amounts to $\sim 10^{10}$ free parameters.

V. OUTLOOK

In this work, we introduce a classical variational method for simulating QAOA, a hybrid quantum-classical approach for solving combinatorial optimizations with prospects of quantum speedup on near-term devices. To the best of our knowledge, this technique is the first self-contained approximate simulator based on NQS methods borrowed from many-body quantum physics, departing from the exponentially-scaling exact simulations of this class of quantum circuits.

We successfully explore previously unreachable regions in the QAOA parameter space, owing to heuristically sub-exponential complexity scaling of our method near optimal QAOA angles. Model limitations are discussed in terms of lower fidelities in quantum state reproduction away from said optimum. Because of such different area of applicability and relative low computational cost, the method is introduced as complementary to established numerical methods of classical simulation of quantum circuits.

Classical variational simulations of quantum algorithms provide a natural way to both benchmark and

understand the limitations of near-future quantum hardware. On the algorithmic side, our approach can help answer a fundamentally open question in the field, namely whether QAOA can outperform classical optimization algorithms or quantum-inspired classical algorithms based on artificial neural networks [34, 35].

Code

Our Python code is available on GitHub to reproduce the results presented in this paper.

Acknowledgements

The authors thank S. Bravyi for enlightening discussions. Numerical simulations were performed using NumPy [36], SciPy [37], Google Cirq [38] and PastaQ [39] for MPS simulations. Plots were generated using Matplotlib [40]. MM acknowledges support from the CCQ graduate fellowship in computational quantum physics. The Flatiron Institute is a division of the Simons Foundation.

[1] F. Arute, K. Arya, R. Babbush, D. Bacon, J. C. Bardin, R. Barends, R. Biswas, S. Boixo, F. G. Brandao, D. A. Buell, B. Burkett, Y. Chen, Z. Chen, B. Chiaro, R. Collins, W. Courtney, A. Dunsworth, E. Farhi, B. Foxen, A. Fowler, C. Gidney, M. Giustina, R. Graff, K. Guerin, S. Habegger, M. P. Harrigan, M. J. Hartmann, A. Ho, M. Hoffmann, T. Huang, T. S. Humble, S. V. Isakov, E. Jeffrey, Z. Jiang, D. Kafri, K. Kechedzhi, J. Kelly, P. V. Klimov, S. Knysh, A. Korotkov, F. Kostritsa, D. Landhuis, M. Lindmark, E. Lucero, D. Lyakh, S. Mandrà, J. R. McClean, M. McEwen, A. Megrant, X. Mi, K. Michelsen, M. Mohseni, J. Mutus, O. Naaman, M. Neeley, C. Neill, M. Y. Niu, E. Ostby, A. Petukhov, J. C. Platt, C. Quintana, E. G. Rieffel, P. Roushan, N. C. Rubin, D. Sank, K. J. Satzinger, V. Smelyanskiy, K. J. Sung, M. D. Trevithick, A. Vainsencher, B. Villalonga, T. White, Z. J. Yao, P. Yeh, A. Zalcman, H. Neven, and J. M. Martinis, “Quantum supremacy using a programmable superconducting processor,” *Nature* **574** no. 7779, (Oct, 2019) 505–510.

[2] J. Preskill, “Quantum Computing in the NISQ era and beyond,” *Quantum* **2** (2018) 79. <https://quantum-journal.org/papers/q-2018-08-06-79/>.

[3] A. Peruzzo, J. McClean, P. Shadbolt, M. H. Yung, X. Q. Zhou, P. J. Love, A. Aspuru-Guzik, and J. L. O’Brien, “A variational eigenvalue solver on a photonic quantum processor,” *Nature Communications* **5** no. 1, (Jul, 2014) 1–7.

[4] E. Farhi and H. Neven, “Classification with Quantum Neural Networks on Near Term Processors,” [arXiv:1802.06002](https://arxiv.org/abs/1802.06002). [http://arxiv.org/abs/1802.06002](https://arxiv.org/abs/1802.06002).

[5] E. Farhi, J. Goldstone, and S. Gutmann, “A Quantum Approximate Optimization Algorithm,” [arXiv:1411.4028](https://arxiv.org/abs/1411.4028). <http://arxiv.org/abs/1411.4028>.

[6] E. Grant, M. Benedetti, S. Cao, A. Hallam, J. Lockhart, V. Stojevic, A. G. Green, and S. Severini, “Hierarchical quantum classifiers,” *npj Quantum Information* **4** no. 1, (Dec, 2018) 1–8, [arXiv:1804.03680](https://arxiv.org/abs/1804.03680).

[7] Z. Wang, S. Hadfield, Z. Jiang, and E. G. Rieffel, “Quantum approximate optimization algorithm for MaxCut: A fermionic view,” *Physical Review A* **97** no. 2, (Feb, 2018) 022304.

[8] E. Farhi, J. Goldstone, and S. Gutmann, “A Quantum Approximate Optimization Algorithm Applied to a Bounded Occurrence Constraint Problem,” [arXiv:1412.6062](https://arxiv.org/abs/1412.6062). <http://arxiv.org/abs/1412.6062>.

[9] S. Lloyd, “Quantum approximate optimization is computationally universal,” [arXiv:1812.11075](https://arxiv.org/abs/1812.11075). <http://arxiv.org/abs/1812.11075>.

[10] Z. Jiang, E. G. Rieffel, and Z. Wang, “Near-optimal quantum circuit for Grover’s unstructured search using a transverse field,” *Physical Review A* **95** no. 6, (Jun, 2017) 062317, [arXiv:1702.02577](https://arxiv.org/abs/1702.02577).

[11] S. Hadfield, Z. Wang, B. O’Gorman, E. Rieffel, D. Venturelli, and R. Biswas, “From the Quantum Approximate Optimization Algorithm to a Quantum Alternating Operator Ansatz,” *Algorithms* **12** no. 2, (Feb, 2019) 34. [http://www.mdpi.com/1999-4893/12/2/34](https://www.mdpi.com/1999-4893/12/2/34).

[12] L. Zhou, S.-T. Wang, S. Choi, H. Pichler, and M. D. Lukin, “Quantum Approximate Optimization Algorithm: Performance, Mechanism, and Implementation on Near-Term Devices,” *Physical Review X* **10** no. 2, (2020) 021067. <https://arxiv.org/abs/1906.03298>.

//link.aps.org/doi/10.1103/PhysRevX.10.021067.

[13] F. Arute, K. Arya, R. Babbush, D. Bacon, J. C. Bardin, R. Barends, S. Boixo, M. Broughton, B. B. Buckley, D. A. Buell, B. Burkett, N. Bushnell, Y. Chen, Z. Chen, B. Chiaro, R. Collins, W. Courtney, S. Demura, A. Dunsworth, E. Farhi, A. Fowler, B. Foxen, C. Gidney, M. Giustina, R. Graff, S. Habegger, M. P. Harrigan, A. Ho, S. Hong, T. Huang, L. B. Ioffe, S. V. Isakov, E. Jeffrey, Z. Jiang, C. Jones, D. Kafri, K. Kechedzhi, J. Kelly, S. Kim, P. V. Klimov, A. N. Korotkov, F. Kostritsa, D. Landhuis, P. Laptev, M. Lindmark, M. Leib, E. Lucero, O. Martin, J. M. Martinis, J. R. McClean, M. McEwen, A. Megrant, X. Mi, M. Mohseni, W. Mruczkiewicz, J. Mutus, O. Naaman, M. Neeley, C. Neill, F. Neukart, H. Neven, M. Y. Niu, T. E. O'Brien, B. O'Gorman, E. Ostby, A. Petukhov, H. Putterman, C. Quintana, P. Roushan, N. C. Rubin, D. Sank, K. J. Satzinger, A. Skolik, V. Smelyanskiy, D. Strain, M. Streif, K. J. Sung, M. Szalay, A. Vainsencher, T. White, Z. J. Yao, P. Yeh, A. Zalcman, and L. Zhou, "Quantum Approximate Optimization of Non-Planar Graph Problems on a Planar Superconducting Processor," [arXiv:2004.04197](https://arxiv.org/abs/2004.04197). <http://arxiv.org/abs/2004.04197>.

[14] G. E. Santoro, R. Martoňák, E. Tosatti, and R. Car, "Theory of Quantum Annealing of an Ising Spin Glass," *Science* **295** no. 5564, (Mar., 2002) 2427–2430. <http://science.sciencemag.org/content/295/5564/2427>.

[15] T. F. Rønnow, Z. Wang, J. Job, S. Boixo, S. V. Isakov, D. Wecker, J. M. Martinis, D. A. Lidar, and M. Troyer, "Defining and detecting quantum speedup," *Science* **345** no. 6195, (July, 2014) 420–424. <http://science.sciencemag.org/content/345/6195/420>.

[16] G. G. Guerreschi and A. Y. Matsuura, "QAOA for Max-Cut requires hundreds of qubits for quantum speed-up," *Scientific Reports* **9** no. 1, (Dec, 2019) 1–7, [arXiv:1812.07589](https://arxiv.org/abs/1812.07589).

[17] G. Pagano, A. Bapat, P. Becker, K. S. Collins, A. De, P. W. Hess, H. B. Kaplan, A. Kyprianidis, W. L. Tan, C. Baldwin, L. T. Brady, A. Deshpande, F. Liu, S. Jordan, A. V. Gorshkov, and C. Monroe, "Quantum Approximate Optimization of the Long-Range Ising Model with a Trapped-Ion Quantum Simulator," [arXiv:1906.02700](https://arxiv.org/abs/1906.02700). <http://arxiv.org/abs/1906.02700>.

[18] A. Bengtsson, P. Vikstål, C. Warren, M. Svensson, X. Gu, A. F. Kockum, P. Krantz, C. Križan, D. Shiri, I.-M. Svensson, G. Tancredi, G. Johansson, P. Delsing, G. Ferrini, and J. Bylander, "Quantum approximate optimization of the exact-cover problem on a superconducting quantum processor," [arXiv:1912.10495](https://arxiv.org/abs/1912.10495). <http://arxiv.org/abs/1912.10495>.

[19] M. Willsch, D. Willsch, F. Jin, H. De Raedt, and K. Michielsen, "Benchmarking the quantum approximate optimization algorithm," *Quantum Information Processing* **19** no. 7, (Jul, 2020) 1–24, [arXiv:1907.02359](https://arxiv.org/abs/1907.02359).

[20] J. S. Otterbach, R. Manenti, N. Alidoust, A. Bestwick, M. Block, B. Bloom, S. Caldwell, N. Didier, E. S. Fried, S. Hong, P. Karalekas, C. B. Osborn, A. Papageorge, E. C. Peterson, G. Prawiroatmodjo, N. Rubin, C. A. Ryan, D. Scarabelli, M. Scheer, E. A. Sete, P. Sivarajah, R. S. Smith, A. Staley, N. Tezak, W. J. Zeng,

A. Hudson, B. R. Johnson, M. Reagor, M. P. da Silva, and C. Rigetti, "Unsupervised Machine Learning on a Hybrid Quantum Computer," [arXiv:1712.05771](https://arxiv.org/abs/1712.05771). <http://arxiv.org/abs/1712.05771>.

[21] S. Bravyi, D. Browne, P. Calpin, E. Campbell, D. Gosset, and M. Howard, "Simulation of quantum circuits by low-rank stabilizer decompositions," *Quantum* **3** (Sep, 2019) 181, [arXiv:1808.00128](https://arxiv.org/abs/1808.00128).

[22] G. Carleo and M. Troyer, "Solving the quantum many-body problem with artificial neural networks," *Science* **355** no. 6325, (Feb, 2017) 602–606.

[23] B. Jónsson, B. Bauer, and G. Carleo, "Neural-network states for the classical simulation of quantum computing," [arXiv:1808.05232](https://arxiv.org/abs/1808.05232) (2018) . <http://arxiv.org/abs/1808.05232>. arXiv: 1808.05232.

[24] B. Villalonga, D. Lyakh, S. Boixo, H. Neven, T. S. Humble, R. Biswas, E. G. Rieffel, A. Ho, and S. Mandr, "Establishing the quantum supremacy frontier with a 281 Pflop/s simulation," *Quantum Science and Technology* **5** no. 3, (May, 2020) , [arXiv:1905.00444](https://arxiv.org/abs/1905.00444)<http://dx.doi.org/10.1088/2058-9565/ab7eeb>.

[25] D. P. Kingma and J. L. Ba, "Adam: A method for stochastic optimization," in *3rd International Conference on Learning Representations, ICLR 2015 - Conference Track Proceedings*. International Conference on Learning Representations, ICLR, Dec, 2015. [arXiv:1412.6980](https://arxiv.org/abs/1412.6980).

[26] G. E. Hinton, "Training products of experts by minimizing contrastive divergence," *Neural Computation* **14** no. 8, (Aug, 2002) 1771–1800.

[27] G. E. Hinton and R. R. Salakhutdinov, "Reducing the dimensionality of data with neural networks," *Science* **313** no. 5786, (Jul, 2006) 504–507.

[28] Y. Lecun, Y. Bengio, and G. Hinton, "Deep learning," May, 2015.

[29] S. Sorella, "Green function monte carlo with stochastic reconfiguration," *Physical Review Letters* **80** no. 20, (May, 1998) 4558–4561, [arXiv:9803107](https://arxiv.org/abs/9803107) [cond-mat].

[30] S. R. White, "Density matrix formulation for quantum renormalization groups," *Physical Review Letters* **69** no. 19, (Nov, 1992) 2863–2866.

[31] G. Vidal, "Efficient classical simulation of slightly entangled quantum computations," *Physical Review Letters* **91** no. 14, (Oct, 2003) 147902, [arXiv:0301063](https://arxiv.org/abs/0301063) [quant-ph].

[32] G. Vidal, "Efficient simulation of one-dimensional quantum many-body systems," *Physical Review Letters* **93** no. 4, (Jul, 2004) 040502, [arXiv:0310089](https://arxiv.org/abs/0310089) [quant-ph]. <https://journals.aps.org/prl/abstract/10.1103/PhysRevLett.93.040502>.

[33] Y. Zhou, E. M. Stoudenmire, and X. Waintal, "What limits the simulation of quantum computers?" [arXiv:2002.07730](https://arxiv.org/abs/2002.07730) [cond-mat, physics:quant-ph] (Mar., 2020) . <http://arxiv.org/abs/2002.07730>.

[34] J. Gomes, K. A. McKiernan, P. Eastman, and V. S. Pande, "Classical Quantum Optimization with Neural Network Quantum States," [arXiv:1910.10675](https://arxiv.org/abs/1910.10675) (Oct., 2019) . <http://arxiv.org/abs/1910.10675>.

[35] T. Zhao, G. Carleo, J. Stokes, and S. Veerapaneni, "Natural evolution strategies and quantum approximate optimization," [arXiv:2005.04447](https://arxiv.org/abs/2005.04447) (2020) . <http://arxiv.org/abs/2005.04447>.

- [36] S. Van Der Walt, S. C. Colbert, and G. Varoquaux, “The NumPy array: A structure for efficient numerical computation,” *Computing in Science and Engineering* **13** no. 2, (2011) 22–30.
- [37] P. Virtanen, R. Gommers, and T. E. e. a. Oliphant, “SciPy 1.0: fundamental algorithms for scientific computing in Python,” *Nature Methods* **17** no. 3, (Mar, 2020) 261–272, [arXiv:1907.10121](https://arxiv.org/abs/1907.10121). <https://doi.org/10.1038/s41592-019-0686-2>.
- [38] C. Gidney, D. Bacon, and The Cirq Developers, “quantumlib/Cirq: A python framework for creating, editing, and invoking Noisy Intermediate Scale Quantum (NISQ) circuits.,” 2018. <https://github.com/quantumlib/Cirq>.
- [39] G. Torlai, M. Stoudenmire, and M. Fishman, “PastaQ.jl: Package for Simulation, Tomography and Analysis of Quantum Computers,” 2020. <https://github.com/GTorlai/PastaQ.jl>.
- [40] J. D. Hunter, “Matplotlib: A 2D graphics environment,” *Computing in Science and Engineering* **9** no. 3, (2007) 99–104.
- [41] J. Stokes, J. Izaac, N. Killoran, and G. Carleo, “Quantum Natural Gradient,” *Quantum* **4** (May, 2020) 269. <https://quantum-journal.org/papers/q-2020-05-25-269/>. Publisher: Verein zur Förderung des Open Access Publizierens in den Quantenwissenschaften.
- [42] S.-i. Amari, “Natural Gradient Works Efficiently in Learning,” *Neural Computation* **10** no. 2, (Feb., 1998) 251–276. <http://www.mitpressjournals.org/doi/10.1162/089976698300017746>.
- [43] N. Metropolis, A. W. Rosenbluth, M. N. Rosenbluth, A. H. Teller, and E. Teller, “Equation of state calculations by fast computing machines,” *The Journal of Chemical Physics* **21** no. 6, (1953) 1087–1092.
- [44] W. K. Hastings, “Monte carlo sampling methods using Markov chains and their applications,” *Biometrika* **57** no. 1, (1970) 97–109.
- [45] M. E. J. Newman and G. T. Barkema, “Monte Carlo Methods in Statistical Physics,” *Oxford University Press* (1999) .
- [46] G. Carleo, F. Becca, M. Schiro, and M. Fabrizio, “Localization and Glassy Dynamics Of Many-Body Quantum Systems,” *Scientific Reports* **2** (Feb., 2012) 243.

Appendix A: Exact gate application to Restricted Boltzmann Machines

In this section we enumerate the one- and two-qubit gates that can be exactly applied to the variational RBM ansatz given in Eq. 4.

1. One-qubit Pauli gates

Parameter replacement rules we use to directly apply one-qubit gates can be obtained directly by solving Eq. 5.

a. Pauli X gate

The Pauli X_i or NOT_i gate acting on qubit i can be applied by satisfying the following system of equations:

$$\begin{aligned} \ln C + a'_i B_i &= (1 - B_i) a_i \\ b'_k + B_i W'_{ik} &= b_k + (1 - B_i) W_{ik} . \end{aligned} \tag{A1}$$

for $B_i = 0, 1$. The solution is:

$$\ln C = a_i ; \quad a'_i = -a_i ; \quad b'_k = b_k + W_{ik} ; \quad W'_{ik} = -W_{ik} , \tag{A2}$$

with all other parameters remaining unchanged.

b. Pauli Y gate

A similar solution can be found for the Pauli Y gate:

$$\ln C = a_i + \frac{i\pi}{2} ; \quad a'_i = -a_i + i\pi ; \quad b'_k = b_k + W_{ik} ; \quad W'_{ik} = -W_{ik} , \tag{A3}$$

with all other parameters remaining unchanged as well.

c. *Pauli Z gate*

As described in the main text, one needs to solve $e^{a'_i B_i} = (-1)^{B_i} e^{a_i B_i}$. The solution is simply

$$a'_i = a_i + i\pi . \quad (\text{A4})$$

d. *Z rotations*

The Z rotation gate is given in matrix form as:

$$RZ(\varphi) = e^{-i\frac{\varphi}{2}Z} \propto \begin{pmatrix} 1 & 0 \\ 0 & e^{i\varphi} \end{pmatrix} \quad (\text{A5})$$

where the proportionality is up to a global phase factor. Similar to the Pauli Z_i gate, this gate can be implemented on qubit i by solving $e^{a'_i B_i} = e^{i\varphi B_i} e^{a_i B_i}$. The solution is simply:

$$a'_i = a_i + i\varphi , \quad (\text{A6})$$

with all other parameters besides a_i remaining unchanged. This expression reduces to the Pauli Z gate replacement rules for $\varphi = \pi$ as required.

2. Two-qubit gates

We apply two-qubit gates between qubits k and l by adding an additional hidden unit (labeled by c) to the RBM before solving Eq. 5. The extra hidden unit couples only to qubits in question, leaving all previously existing parameters unchanged. In that special case, the equation reduces to

$$e^{\Delta a_k B_k + \Delta a_l B_l} (1 + e^{W_{kc} B_k + W_{lc} B_l}) \psi_\theta(\mathcal{B}) = C \langle \mathcal{B} | \mathcal{G} | \psi_\theta \rangle . \quad (\text{A7})$$

a. *ZZ rotations*

The ZZ rotation matrix RZZ is key for being able to implement the first step in the QAOA algorithm. The definition is:

$$RZZ(\varphi) = e^{-i\frac{\varphi}{2}Z \otimes Z} \propto \begin{pmatrix} 1 & 0 & 0 & 0 \\ 0 & e^{i\varphi} & 0 & 0 \\ 0 & 0 & e^{i\varphi} & 0 \\ 0 & 0 & 0 & 1 \end{pmatrix} , \quad (\text{A8})$$

where the proportionality factor is again a global phase. The related matrix element for a RZZ_{kl} gate between qubits k and l is $\langle B'_k B'_l | RZZ_{kl}(\varphi) | B_k B_l \rangle = e^{i\varphi B_k \vee B_l}$ where \vee stands for the classical exclusive or (XOR) operation. Then, one solution to Eq. A7 reads:

$$\begin{aligned} W_{ic} &= -2\mathcal{A}(\varphi) ; & W_{jc} &= 2\mathcal{A}(\varphi) \\ a'_i &= a_i + \mathcal{A}(\varphi) ; & a'_j &= a_j - \mathcal{A}(\varphi) , \end{aligned} \quad (\text{A9})$$

where $\mathcal{A}(\varphi) = \text{Arccosh}(e^{i\varphi})$ and $C = 2$.

b. *Controlled Z rotations*

The controlled Z rotation matrix CRZ is defined as:

$$CRZ(\varphi) = \begin{pmatrix} 1 & 0 & 0 & 0 \\ 0 & 1 & 0 & 0 \\ 0 & 0 & 1 & 0 \\ 0 & 0 & 0 & e^{i\varphi} \end{pmatrix}, \quad (\text{A10})$$

Similar to the RZZ case, the replacement rules read:

$$\begin{aligned} W_{kc} &= -2\mathcal{A}'(\varphi); & W_{lc} &= 2\mathcal{A}'(\varphi) \\ a'_k &= a_k + \frac{i\varphi}{2} + \mathcal{A}'(\varphi); & a'_l &= a_l + \frac{i\varphi}{2} - \mathcal{A}'(\varphi) \end{aligned} \quad (\text{A11})$$

where $\mathcal{A}'(\varphi) = \text{Arccosh}(e^{-i\varphi/2})$ and $C = 2$ as well.

Appendix B: Model and optimization details

In this section we provide model details and show how to approximately apply quantum gates that cannot be implemented through methods described in Sec. A. Furthermore, we discuss the connection of our model to the time-dependent Variational Monte Carlo (t-VMC) computational technique commonly used in many-body quantum physics in Appendix D.

1. Approximate gate application

In this work we use the Stochastic Reconfiguration (SR) [29] algorithm to approximately apply quantum gates to the RBM ansatz. To that end, we write the "infidelity" between our RBM ansatz and the target state ϕ , $\mathcal{D}(\psi_\theta, \phi) = 1 - F(\psi_\theta, \phi)$, as an expectation value of an effective hamiltonian operator H_{eff}^ϕ :

$$\mathcal{D}(\psi_\theta, \phi) = \frac{\langle \psi_\theta | H_{\text{eff}}^\phi | \psi_\theta \rangle}{\langle \psi_\theta | \psi_\theta \rangle} \quad \rightarrow \quad H_{\text{eff}}^\phi = \mathbb{1} - \frac{|\phi\rangle\langle\phi|}{\langle\phi|\phi\rangle} \quad (\text{B1})$$

We call the hermitian operator given in Eq. B1 a "hamiltonian" only because the target quantum state $|\psi\rangle$ is encoded into it as the eigenstate corresponding to the smallest eigenvalue. Our optimization scheme focuses on finding small parameter updates Δ_k that locally approximate the action of the imaginary time evolution operator associated with H_{eff}^ϕ , thus filtering out the target state:

$$|\psi_{\theta+\Delta}\rangle \stackrel{!}{=} C e^{-\eta H} |\psi_\theta\rangle, \quad (\text{B2})$$

where C is an arbitrary constant included because our variational states (Eq. 4) are not normalized. Choosing both η and Δ to be small, one can expand both sides to linear order in those variables and solve the resulting linear system for all components of Δ , after eliminating C first. After some simplification, one arrives at the following parameter at each loop iteration (indexed with t):

$$\theta_k^{(t+1)} = \theta_k^{(t)} - \eta \sum_l S_{kl}^{-1} \frac{\partial \mathcal{D}}{\partial \theta_l^*}, \quad (\text{B3})$$

where stochastic estimations of gradients of the cost function $\mathcal{D}(\psi_\theta, \phi)$ can be obtained through samples from $|\psi_\theta|^2$ at each loop iteration through:

$$\frac{\partial \mathcal{D}}{\partial \theta_k^*} = \left\langle \mathcal{O}_k^\dagger H_{\text{eff}}^\phi \right\rangle_{\psi_\theta} - \left\langle \mathcal{O}_k^\dagger \right\rangle_{\psi_\theta} \left\langle H_{\text{eff}}^\phi \right\rangle_{\psi_\theta}. \quad (\text{B4})$$

Here, \mathcal{O}_k is defined as a diagonal operator in the computational basis such that $\langle \mathcal{B}' | \mathcal{O}_k | \mathcal{B} \rangle = \frac{\partial \ln \psi_\theta}{\partial \theta_k} \delta_{\mathcal{B}' \mathcal{B}}$. Averages over ψ_θ are commonly defined as $\langle \cdot \rangle_\psi \equiv \langle \psi | \cdot | \psi \rangle / \langle \psi | \psi \rangle$. Furthermore, the S -matrix appearing in Eq. B3 reads:

$$S_{kl} = \left\langle \mathcal{O}_k^\dagger \mathcal{O}_l \right\rangle_{\psi_\theta} - \left\langle \mathcal{O}_k^\dagger \right\rangle_{\psi_\theta} \left\langle \mathcal{O}_l \right\rangle_{\psi_\theta}, \quad (\text{B5})$$

and corresponds to the Quantum Geometric Tensor or Quantum Fisher Information (also see Ref. [41] for a detailed description and connection with the natural gradient method in classical machine learning [42]).

Exact computations of averages over N qubit states ψ_θ and ϕ at each optimization step range from impractical to intractable, even for moderate N . Therefore, we evaluate those averages by importance-sampling the probability distributions associated with the variational ansatz $|\psi_\theta|^2$ and the target state $|\phi|^2$ at each optimization step t . All of the above expectation values are evaluated using Markov Chain Monte Carlo (MCMC) [43, 44] sampling with basic single-spin flip local updates. An overview of the sampling method can be found in [45]. In order to use those techniques, we rewrite Eq. B4 as:

$$\frac{\partial \mathcal{D}}{\partial \theta_l^*} = \left\langle \frac{\phi}{\psi_\theta} \right\rangle_{\psi_\theta} \left\langle \frac{\psi_\theta}{\phi} \right\rangle_\phi \left[\left\langle \mathcal{O}_k^* \right\rangle_{\psi_\theta} - \frac{\left\langle \frac{\phi}{\psi_\theta} \mathcal{O}_k^* \right\rangle_{\psi_\theta}}{\left\langle \frac{\phi}{\psi_\theta} \right\rangle_{\psi_\theta}} \right]. \quad (\text{B6})$$

The entire Eq. B6 is manifestly invariant to rescaling of ψ_θ and ϕ , removing the need to ever compute normalization constants.

The second step consists of multiplying the variational derivative with the inverse of the S -matrix (Eq. B5) corresponding to a stochastic estimation of a metric tensor on the hermitian parameter manifold. Thereby, the usual gradient is transformed into the natural gradient on that manifold. However, the S -matrix is stochastically estimated and it can happen that it is singular. To regularize it, we replace S with $S + \epsilon \mathbb{1}$, ensuring that the resulting linear system has a unique solution. We choose $\epsilon = 10^{-3}$ throughout.

The optimization procedure is summarized by the following algorithm:

Algorithm 1: Target state approximation with an RBM.

Input: Initial parameters θ , target state ϕ , target fidelity tolerance tol , learning rate η

Result: Parameters $\theta' = \{\mathbf{a}', \mathbf{b}', W'\}$ such that $|\psi_{\theta'}\rangle \approx |\phi\rangle$

$\partial_k \ln F \leftarrow 0$; $S_{kl} \leftarrow 0$; $\theta' \leftarrow \theta$;

while $F < 1 - \text{tol}$ **do**

 Generate samples $\mathcal{B}_\psi \sim |\psi_{\theta'}|^2$ and $\mathcal{B}_\phi \sim |\phi|^2$ using MCMC;

foreach \mathcal{B} in \mathcal{B}_ψ **do** evaluate and store $\psi_{\theta'}(\mathcal{B})$, $\phi(\mathcal{B})$ and $\mathcal{O}_k(\mathcal{B})$ for all parameters ;

foreach \mathcal{B} in \mathcal{B}_ϕ **do** evaluate and store $\psi_{\theta'}(\mathcal{B})$ and $\phi(\mathcal{B})$;

 evaluate and set $F \leftarrow \text{Re} \left\{ \left\langle \frac{\phi(\mathcal{B})}{\psi(\mathcal{B})} \right\rangle_{\mathcal{B} \sim \mathcal{B}_\psi} \left\langle \frac{\psi(\mathcal{B})}{\phi(\mathcal{B})} \right\rangle_{\mathcal{B} \sim \mathcal{B}_\phi} \right\}$;

foreach k **do** evaluate and set $\partial_k \ln F \leftarrow \left\langle \mathcal{O}_k^* \right\rangle_{\mathcal{B} \sim \mathcal{B}_\psi} - \left\langle \frac{\phi}{\psi_\theta} \mathcal{O}_k^* \right\rangle_{\mathcal{B} \sim \mathcal{B}_\psi} / \left\langle \frac{\phi}{\psi_\theta} \right\rangle_{\mathcal{B} \sim \mathcal{B}_\psi}$;

foreach k, l **do** evaluate and set $S_{kl} \leftarrow \left\langle \mathcal{O}_k^\dagger \mathcal{O}_l \right\rangle_{\psi_\theta} - \left\langle \mathcal{O}_k^\dagger \right\rangle_{\psi_\theta} \left\langle \mathcal{O}_l \right\rangle_{\psi_\theta}$;

 solve linear system $\sum_l S_{kl} \Delta_l = F \times \partial_k \ln F$;

foreach k **do** $\theta'_k \leftarrow \theta'_k - \eta \Delta_k$;

end

return θ'

2. Model compression

As outlined in the main text, in order to keep the number of hidden units reasonable, we employ a *compression* step at each QAOA layer (after the first). Immediately after applying the $U_C(\gamma_i)$ gate in layer i to the RBM ψ_θ (and thereby introducing the unwanted parameters), we go through the following steps:

1. Construct a new RBM $\tilde{\psi}_\theta$.
2. Initialize $\tilde{\psi}_\theta$ to exactly represent the state $U_C \left(\sum_{j \leq i} \gamma_j \right) |+\rangle$. Doing this introduces half the number hidden units that are already present in the ψ_θ .

3. Stochastically optimize $\tilde{\psi}_\theta$ to approximate ψ_θ using Algorithm 1 with $\phi \rightarrow \psi_\theta$ and $\psi \rightarrow \tilde{\psi}_\theta$.

In essence, we use Algorithm 1 with the "larger" ψ_θ as the target state ϕ . The optimization results in a new RBM state with fewer hidden units that closely approximates the old RBM with fidelity > 0.98 in all our tests. We then proceed to simulate the rest of the QAOA circuit and apply the same compression procedure again when the number of parameters increases again. The exact schedule of applying this procedure in context of different QAOA layers can be seen on Fig. 1.

Initial state for the optimization was chosen as an exactly reproducible RBM state that has non-zero overlap with the target (larger) RBM. In principle, any other such state would work, but we heuristically found this one to be a reliable choice across all p values studied.

Appendix C: Exact $p=1$ formula

In this section we present the exact MaxCut QAOA cost formula used for quantifying the accuracy of our model result.

Theorem 1 *For an arbitrary graph G , the QAOA cost function for the MaxCut problem given in Eq. 3 takes the form*

$$C(\gamma, \beta) = \frac{1}{2} \sum_{\langle k, l \rangle} \left[\sin(4\beta) \sin(2\gamma) (\cos^{q_k}(2\gamma) + \cos^{q_l}(2\gamma)) + \sin^2(2\beta) \cos^{q_k+q_l-2\Delta_{kl}}(2\gamma) (1 - \cos^{\Delta_{kl}}(4\gamma)) \right] \quad (\text{C1})$$

at $p = 1$. Here, $q_k + 1$ and $q_l + 1$ are degrees of vertices k and l and Δ_{kl} is the number of common neighbors between those vertices.

Proof: The proof repeats much of what has already been done in [7]. We begin by expressing the density operator associated with the $|+\rangle$ state as

$$\rho_0 = |+\rangle\langle+| = \prod_i \frac{\mathbb{1}_i + X_i}{2} . \quad (\text{C2})$$

Then, we can express the MaxCut QAOA cost function at $p = 1$ as

$$\langle \gamma, \beta | \mathcal{C} | \gamma, \beta \rangle = \sum_{\langle k, l \rangle} \text{Tr} \left[\rho_0 U_C^\dagger(\gamma) U_B^\dagger(\beta) Z_k Z_l U_B(\beta) U_C(\gamma) \right] \quad (\text{C3})$$

In what follows, we will make repeated use of the following identities:

$$e^{i\beta X} Z e^{-i\beta X} = \cos(2\beta) Z + \sin(2\beta) Y \quad (\text{C4})$$

$$e^{-i\gamma Z \otimes Z} = \cos \gamma - i \sin \gamma Z \otimes Z \quad (\text{C5})$$

$$e^{-i\gamma Z} Y = Y e^{i\gamma Z} . \quad (\text{C6})$$

The innermost product can easily be expanded using Eq. C4 twice:

$$\begin{aligned} U_B^\dagger(\beta) Z_k Z_l U_B(\beta) &= U_B^\dagger(\beta) Z_k U_B(\beta) U_B^\dagger(\beta) Z_l U_B(\beta) = \\ &= \cos^2(2\beta) Z_k Z_l + \frac{1}{2} \sin(4\beta) (Y_k Z_l + Y_l Z_k) + \cos^2(2\beta) Y_k Y_l . \end{aligned} \quad (\text{C7})$$

The first term vanishes when averaged against ρ_0 . The second and third need to be treated separately. First we look at expressions of the form:

$$\text{Tr} \left[\rho_0 e^{i\gamma \mathcal{C}} Y_k Z_l e^{-i\gamma \mathcal{C}} \right] = \text{Tr} \left[\rho_0 Y_k Z_l \prod_{j \in N(k)} e^{-2i\gamma Z_k Z_j} \right] = \text{Tr} \left[\rho_0 Y_k Z_l \prod_{j \in N(k)} (\cos 2\gamma - i \sin 2\gamma Z_k Z_j) \right] , \quad (\text{C8})$$

where we denoted the set of all neighbors of node k by $N(k)$ used Eq. C6 and Eq. C5. In Eq. C8, tracing out Paulis not associated to either node k or its neighbors is trivial and produces a factor of unity. Furthermore, tracing out immediate neighbors of k other than l produces a factor of $\cos^{q_k}(2\gamma)$ where $q_k + 1$ is the degree of node k . Keeping those factors aside, we are left with:

$$\text{Tr}_{kl} \left[\frac{\mathbb{1}_k + X_k}{2} \frac{\mathbb{1}_l + X_l}{2} Y_k Z_l (\cos 2\gamma - i \sin 2\gamma Z_k Z_l) \right] = \sin 2\gamma. \quad (\text{C9})$$

Therefore, the final contribution from the second term in Eq. C7 is

$$\frac{1}{2} \sin(4\beta) \text{Tr} [\rho_0 e^{i\gamma\mathcal{C}} (Y_k Z_l + Y_l Z_k) e^{-i\gamma\mathcal{C}}] = \frac{1}{2} \sin(2\gamma) \sin(4\beta) [\cos^{q_k}(2\gamma) + \cos^{q_l}(2\gamma)] \quad (\text{C10})$$

Looking at the last factor in Eq. C7, we compute:

$$\begin{aligned} \text{Tr} [\rho_0 e^{i\gamma\mathcal{C}} Y_k Y_l e^{-i\gamma\mathcal{C}}] &= \text{Tr} \left[\rho_0 Y_k Y_l \left(\prod_{\substack{j \in N(k) \\ j \neq l}} e^{-i\gamma Z_k Z_j} \right) \left(\prod_{\substack{i \in N(l) \\ i \neq k}} e^{-i\gamma Z_k Z_i} \right) e^{i\gamma Z_k Z_l} e^{-i\gamma\mathcal{C}} \right] = \\ &= \text{Tr} \left[\rho_0 Y_k Y_l \left(\prod_{\substack{j \in N(k) \\ j \neq l}} e^{-2i\gamma Z_k Z_j} \right) \left(\prod_{\substack{i \in N(l) \\ i \neq k}} e^{-2i\gamma Z_k Z_i} \right) \right], \end{aligned} \quad (\text{C11})$$

where we separated factor in \mathcal{C} corresponding to the edge (k, l) out before using Eq. C6. In the second equality, the factor corresponding to the edge (k, l) was canceled and others were absorbed into product expressions.

Like before, operators corresponding to nodes other than k or l or their neighbors can be traced out trivially. The next step is to trace out Paulis that are neighbors of k but not l . Each of those contributes with a factor of $\cos(2\gamma)$ so we get a factor of $\cos^{q_k - \Delta_{kl}}(2\gamma)$ for node k and a corresponding factor for node l resulting in $\cos^{q_k + q_l - 2\Delta_{kl}}(2\gamma)$. Here, we denoted the number of common neighbors of k and l by Δ_{kl} and label their set by $CN(k, l)$ in what remains of Eq. C11:

$$\text{Tr} [\rho_0 e^{i\gamma\mathcal{C}} Y_k Y_l e^{-i\gamma\mathcal{C}}] = \cos^{q_k + q_l - 2\Delta_{kl}}(2\gamma) \text{Tr} \left[\rho'_0 Y_k Y_l \prod_{i \in CN(k, l)} (e^{-2i\gamma Z_k Z_i} e^{-2i\gamma Z_l Z_i}) \right], \quad (\text{C12})$$

where ρ'_0 is the reduced density operator. Using Eq. C5, one can trace out nodes in $CN(k, l)$ to obtain a factor of $(\cos^2 2\gamma + \sin^2 2\gamma Z_k Z_l)^{\Delta_{kl}}$. Finally, we expand that expression using the binomial theorem and interchange the trace operation with the sum. The trace in Eq. C12 becomes

$$\cos^{2\Delta_{kl}}(2\gamma) \sum_{\substack{n=0 \\ \text{odd } n}}^{\Delta_{kl}} \binom{\Delta_{kl}}{n} \tan^{2n}(2\gamma) = \frac{1}{2} (1 - \cos^{\Delta_{kl}}(4\gamma)) \quad (\text{C13})$$

Putting all of the ingredients together, we have:

$$C(\gamma, \beta) = \frac{1}{2} \sum_{\langle k, l \rangle} \left[\sin(4\beta) \sin(2\gamma) (\cos^{q_k}(2\gamma) + \cos^{q_l}(2\gamma)) + \sin^2(2\beta) \cos^{q_k + q_l - 2\Delta_{kl}}(2\gamma) (1 - \cos^{\Delta_{kl}}(4\gamma)) \right] \quad (\text{C14})$$

Appendix D: Relation to t-VMC

Time-dependent Variational Monte Carlo (t-VMC) [46] is a numerical technique used in many-body quantum physics to approximately capture time evolution of an arbitrary state often captured by the unitary operator e^{-iHt} associated with the system hamiltonian H . The starting point of such calculations is often almost identical to Eq. B2:

$$|\psi_{\theta(t+\Delta t)}\rangle \stackrel{!}{=} C e^{-iH\Delta t} |\psi_{\theta(t)}\rangle , \quad (\text{D1})$$

after defining an appropriate variational ansatz ψ_θ , usually by defining log-derivative operators \mathcal{O}_k , like in the main text of this work. By repeating the calculation outlined in the previous subsection (which in this case is equivalent to plugging into the time-dependent Schrödinger equation), one obtains the so-called optimal equations of motion:

$$\sum_l \langle \mathcal{O}_k^* \mathcal{O}_l \rangle_t^c \dot{\theta}_k(t) = -i \langle \mathcal{O}_k^* H \rangle_t^c , \quad (\text{D2})$$

where $\langle AB \rangle_t^c \equiv \langle AB \rangle_t - \langle A \rangle_t \langle B \rangle_t$ and $\langle \dots \rangle_t \equiv \langle \psi_\theta(t) | \dots | \psi_\theta(t) \rangle / \langle \psi_\theta(t) | \psi_\theta(t) \rangle$. At this point, any standard ODE solver can be employed to propagate parameters θ_k away from the initial condition after using MCMC to stochastically estimate averages $\langle \dots \rangle_t^c$ at each step. We note that t-VMC requires inverting the matrix $\langle \mathcal{O}_k^* \mathcal{O}_l \rangle_t^c$ which is analogous to the S matrix given in Eq. B5 in the main text.

In the case of QAOA, one might wish to approximate the action of $U_B(\beta) = \exp(-i\beta \sum_j X_j)$ by employing t-VMC to "propagate" the relevant parameters in β instead of physical time. That approach would have the benefit of being able to apply the entire U_B gate in small $\Delta\beta$ increments instead of doing it qubit-by-qubit. Indeed, if we take Eq. B6 from the main text and set $|\phi\rangle = e^{-i\Delta\beta X_j} |\psi_\theta\rangle$, we obtain:

$$\frac{\partial \mathcal{D}}{\partial \theta_k^*} = \left(\frac{i}{2} \sin(2\Delta\beta) - \sin^2(\Delta\beta) \left\langle \frac{\psi_\theta^{X_j}}{\psi_\theta} \right\rangle_{\psi_\theta}^* \right) \left[\left\langle \mathcal{O}_k^* \frac{\psi_\theta^{X_j}}{\psi_\theta} \right\rangle_{\psi_\theta} - \langle \mathcal{O}_k^* \rangle_{\psi_\theta} \left\langle \frac{\psi_\theta^{X_j}}{\psi_\theta} \right\rangle_{\psi_\theta} \right] , \quad (\text{D3})$$

where $\psi_\theta^{X_j}(\mathcal{B}) \equiv \langle \mathcal{B} | X_j | \psi_\theta \rangle$. If one expands the first factor to first order in $\Delta\beta$, what is left is exactly the $t-VMC$ parameter update one would obtain by following the t-VMC derivation from the beginning. Therefore, our method is more general than t-VMC for any individual qubit. In addition to generality, it has two other key features:

1. Fidelity $F(\phi, \psi)$ is directly used as a cost function and it is recorded at each optimization step. This provides for a more controlled environment where fidelity is explicitly optimized over rather than implicitly. We can apply as many gradient updates as needed to reach the target fidelity.
2. The computational cost of complete (approximate) application of U_B is similar between the two methods. We report that the explicit fidelity method we used in this work required approximately 30 updates per qubit while t-VMC needed 1000-2000 intermediate β points to reach similar final fidelities on 20-qubit test systems.